Nickel Hydroxide "Stacks of Pancakes" Obtained by the Coupled Effect of Ammonia and Template Agent

Corinne Coudun and Jean-François Hochepied*

Ecole Nationale Supérieure des Mines de Paris, Centre d'Energétique, Laboratoire des Systèmes Colloïdaux dans les Procédés Industriels, 60 bd St-Michel, 75006 Paris, France

Received: July 28, 2004; In Final Form: February 3, 2005

The coupled effect of a homemade nickel di-dodecyl sulfate precursor and a complexing base leads to β-Ni(OH)$_2$ "stack of pancakes" morphology. The mean diameter and thickness of the stacks are around 300 and 200 nm, respectively. Moreover, the amount of ammonia not only monitors crystalline structure but also the size and the shape of particles.

Introduction

Nickel hydroxide, Ni(OH)$_2$, is the active material of the positive electrode in alkaline rechargeable batteries (Ni−Cd, Ni−Zn, Ni−Fe, and Ni−MH storage batteries),[1−3] and can also be used as a precursor for catalysts and NiO, well-known for catalytic and electrochromic properties.[4] Two polymorphic forms of nickel hydroxide can be distinguished. The hexagonal β phase is brucite-like (c = 4.60 Å, a = 3.12 Å) and consists of an ordered stacking of well-oriented Ni(OH)$_2$ layers that are 4.60 Å distant, without any intercalated species. The observed morphology for β-Ni(OH)$_2$ is usually hexagonal platelets with a diameter of about 200 nm.[5,6] The α-Ni(OH)$_2$ phase displays more disorder and a larger interlayer spacing (>7.5 Å) as the interlamellar space contains anions (e.g., nitrate, carbonate, sulfate) and water molecules.[7,8] Particles of α-Ni(OH)$_2$[5,6,8,9] are often aggregates of very thin crumpled films. Very recently, Yang et al.[10] reported the synthesis of single-crystalline nanoribbons of Ni(OH)$_2$ displaying a monoclinic lattice and a composition close to the α one. These nanoribbons (length and width about 100 and 5−25 nm, respectively) resulted from the treatment (100 °C for 24 h) of freshly precipitated nickel hydroxide with a high concentration of nickel sulfate.

Controlling size, shape, and crystalline nature of inorganic material enables more efficient products with respect to the future application to be obtained. Such features strongly depend on precipitation conditions and reactant nature. Homogeneous alkalinization makes the control of precipitate's characteristics easier and leads to uniform products. Synthesis from aqueous solutions by decomposition of urea was investigated, leading to submicronic spherical agglomerates[11] or the petal-like shape[12] of α-Ni(OH)$_2$. A complexation followed by complex removal route could also provide a homogeneous precipitation. Besides its basic properties, ammonia displays a strong affinity for cations, such as Ni^{2+}, forming complex. Moreover, additive molecules (surfactant, polymer) could induce a template effect and lead to original and well-controlled morphologies.

Our study investigates the effect of template agent in the presence of ammonia. Instead of simply adding the surfactant to classic nickel salts (e.g., nitrate or sulfate nickel salt) in the bulk, an oil-in-water micellar solution was used, where the metallic cation Ni^{2+} is the counterion of anionic surfactant (dodecyl sulfate). Feltin et al.[13] employed such a method to yield, from ferrous dodecyl sulfate, magnetic nanoparticles whose size was controlled by both temperature and surfactant concentration. Indeed, the bulk where the reaction occurs is free from anions coming from the usual nickel salts (e.g., nitrate or sulfate) and whose presence could be prejudicial for the forthcoming application (remaining NO_3^- anions in nickel oxide electrode lead to corrosion problems). Moreover, beyond the critical micellar concentration (8×10^{-3} mol·L^{-1} for the SDS at 25 °C, and 1.5×10^{-3} mol·L^{-1} for the homemade Ni(DS)$_2$) surfactant molecules form micelles in water.

Experimental Section

Nickel nitrate salt (Ni(NO$_3$)$_2$·6H$_2$O, 97%), nickel sulfate salt (NiSO$_4$·6H$_2$O, 98%), sodium dodecyl sulfate (SDS) ($C_{12}H_{25}$-SO$_4$Na, 96%), and ammonium hydroxide (NH$_4$OH, 28%, d = 0.900) were purchased from Prolabo.

Preparation of the Nickel Precursor Ni(DS)$_2$. The aim of this first step is to associate a surfactant (dodecyl sulfate, $C_{12}H_{25}OSO_3^-$) with the metallic cation Ni^{2+} involved in the precipitation. First, sodium dodecyl sulfate and excess nickel nitrate were dissolved in water at room temperature. Then, the mixture was cooled to 4 °C so that nickel di-dodecyl sulfate, Ni(DS)$_2$, crystallized. Finally, the nickel-functionalized surfactant was washed on büchner with cold water then freeze-dried.

Precipitation of Ni(OH)$_2$. The 1-L reactor consisted of a thermostated hemispheric bottom vessel, equipped with Teflon baffles, that was stirred mechanically at 400 rpm. During the precipitation process, the temperature of the reactor was controlled at 25 or 60 °C (±1 °C). Both temperature and pH in the reactor were recorded by employing a pH-stat PHM290 from Radiometer Analytical. The procedure consisted of two steps. First, at 25 °C, the ammonia (80 mL diluted in 400 mL of distilled water) was injected at a rate of 10 mL/min in the reactor containing the homemade Ni(DS)$_2$ (0.05 mol dissolved in 600 mL of distilled water). During the base injection green nickel hydroxide first precipitated, then it was gradually dissolved to form a blue complex with ammonia, and finally a purple solid containing nickel, ammonia, and dodecyl sulfate appeared. Once the ammonia was completely added, the reaction was remained at 25 °C for 3 h. The second step corresponded to the ammonia removal. By heating at 60 °C, the complexing base was

* Address correspondence to this author. E-mail: hochepied@ensmp.fr. Phone: +331-40-51-91-16. Fax: +331-40-51-94-25.

10.1021/jp0466441 CCC: $30.25
Published on Web 03/08/2005

TABLE 1: Crystallite Lengths Along the (001) and (110) Directions (calculated from XRD patterns applying Scherrer's formula), Mean Thickness and Mean Diameter (measured on TEM patterns) of Sulfate Control Sample, Sample A, and Nickel Hydroxides Precipitated for Different Ammonia Contents (X_{NH_3} = 60, 80, 120, and 160 mL) and for the 60 °C Base Addition Step

	sulfate control sample X_{NH_3} (mL) = 80	sample A X_{NH_3} (mL) = 80	comparison of ammonia conten for X_{NH_3} =				base addition at 60 °C X_{NH_3} (mL) =80
			60	80	120	160	
L_{001} (nm)	15	54	50	51	26	2	48
L_{110} (nm)	28	42	36	39	30	10	38
mean thickness (nm)		200 ± 30	114 ± 24	205 ± 55	-	102 ± 34	86 ± 16
mean diameter (nm)		300 ± 40	374 ± 126	504 ± 95		613 ± 242	320 ± 80

progressively eliminated through a liquid−gas transfer. The precipitation was homogeneous and slow, lasting 23 h. Finally, the precipitate was washed with distilled water and freeze-dried. To keep things clear, the nickel hydroxide synthesized according to the method above is called sample A.

A control sample was precipitated from nickel sulfate salt following the precipitation route described above. At the beginning of the ammonia injection, a green nickel hydroxide also appeared and dissolved to form a blue solution with ammonia. By heating, the medium remained blue until enough ammonia was removed to trigger the precipitation of nickel hydroxide.

Characterization. Scanning electron microscopy (SEM) experiments were performed by using a field effect gun ZEISS DSM 982 LEO Gemini apparatus. Dry powder samples were fixed on carbon tape and coated with 3 nm of gold−palladium. As hydroxides outgas when they are impacted by the beam, charging effects cannot be completely removed. Hence, a low voltage of 2 kV was used as a balance between resolution and the charge effect.

Transmission electron microscopy (TEM) and selected area electron diffraction (SAED) were performed with use of a Phillips EM430 apparatus. Powders were dispersed in distilled water, using an ultrasonic device, and dried in air on carbon-coated copper grids.

Powder X-ray diffraction (XRD) experiments were made on a Bruker D8 diffractometer in $\theta-\theta$ configuration, using cobalt Kα_1 radiation (λ = 1.789 Å) and equipped with a position sensitive detector. Crystallite size was evaluated from the width of isolated lines, applying Scherrer's formula: $L_{hkl} = \{K\lambda\}/\{\Delta_{hkl} \cos\theta\}$, where L_{hkl} is the length of the crystallite along the (hkl) direction, Δ is the full-width at half-maximum of a given [hkl] peak corrected for instrumental broadening and Kα_1 contribution, and λ = 1.789 Å and the structure factor was chosen as K = 0.9.

Results

The Coupled Effect of Nickel Functionalized Surfactant and Ammonia. The XRD pattern of the sulfate control sample (Figure 1a) corresponds to the well-crystallized β-Ni(OH)$_2$ phase (JCPDS no. 14-0117) displaying a hexagonal lattice (a = 3.12 Å and c = 4.62 Å). By applying Scherrer's formula, the length of the crystalline domain along the c-axis (L_{001}) is evaluated at 15 nm and that along the (110) direction (L_{110}) equals 28 nm (Table 1). As revealed by SEM experiments, the sulfate control sample is homogeneous and consists of particles of about 10 μm (Figure 2a). By magnifying, a loose structure becomes apparent as thin and large branched platelets give rise to coarse interstices (Figure 2b).

By substituting nickel sulfate salt by nickel di-dodecyl sulfate, Ni(DS)$_2$, the well-crystallized β phase is also synthesized (Figure 1b). But, the corresponding peaks turned narrower and sharper than in the sulfate sample case: L_{001} and L_{110} reach 54 and 42 nm, respectively (Table 1). Meyer et al.[15] established that the weaker the strength of the base, the narrower the XRD peaks. Hence, nickel hydroxides synthesized with NH_3 are expected to display large coherent crystal domains. Nevertheless, the crystallinity degree of the sample is rather outstanding: generally at low synthesis temperature defects (the stacking faults of brucite layers) are well-known to broaden and modify the shape of the peaks[14] as observed for the sulfate case, and generally hydrothermal conditions are required to obtain well-crystallized particles. Regarding morphology, SEM microscopy reveals that sample A is homogeneous, displaying a denser structure than the sulfate control sample (Figure 2c). The external shape of the particles may be described as regular nanocylinder (Figure 2d).

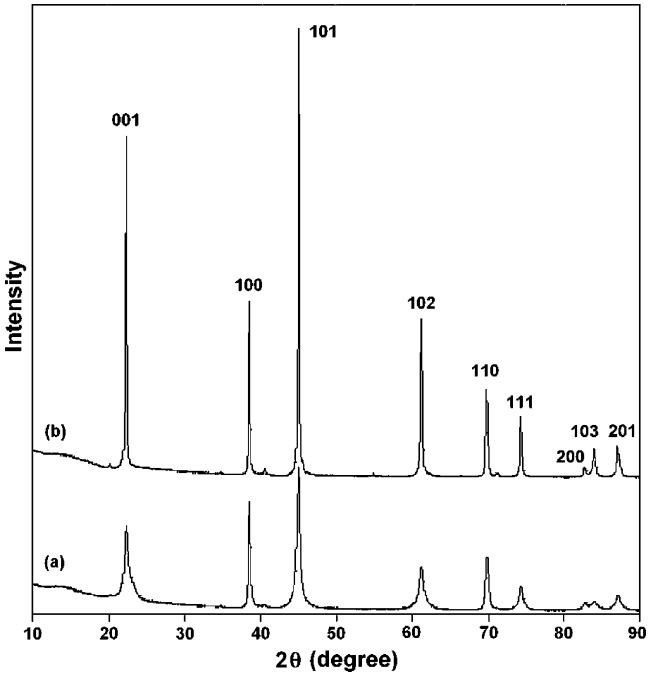

Figure 1. Powder X-ray diffraction patterns of the control sample (a) and the nickel hydroxide β-Ni(OH)$_2$ (sample A) precipitated by ammonia decomplexation (b).

Bright field TEM images (Figure 3a,b) underline not only the homogeneous shape of the sample, but also the lamellar feature of the particles. Each nanocylinder seems to result from the regular stacking of quasicircular platelets. The mean diameter and thickness was measured upon roughly 100 particles on TEM patterns. The mean face diameter is about 300 nm (±40 nm) and the thickness of the stacks is around 200 nm (±30 nm). The enlarged detail of a stack side (Figure 3b) enables the mean thickness of a layer to be estimated at around 3.5 nm. Electron diffraction experiments were carried out on single stacks. Selected area electron diffraction (SAED) performed perpendicularly to the circular face (Figure 3c) displays a hexagonal symmetry revealing that the surface of the stacks is the (001)

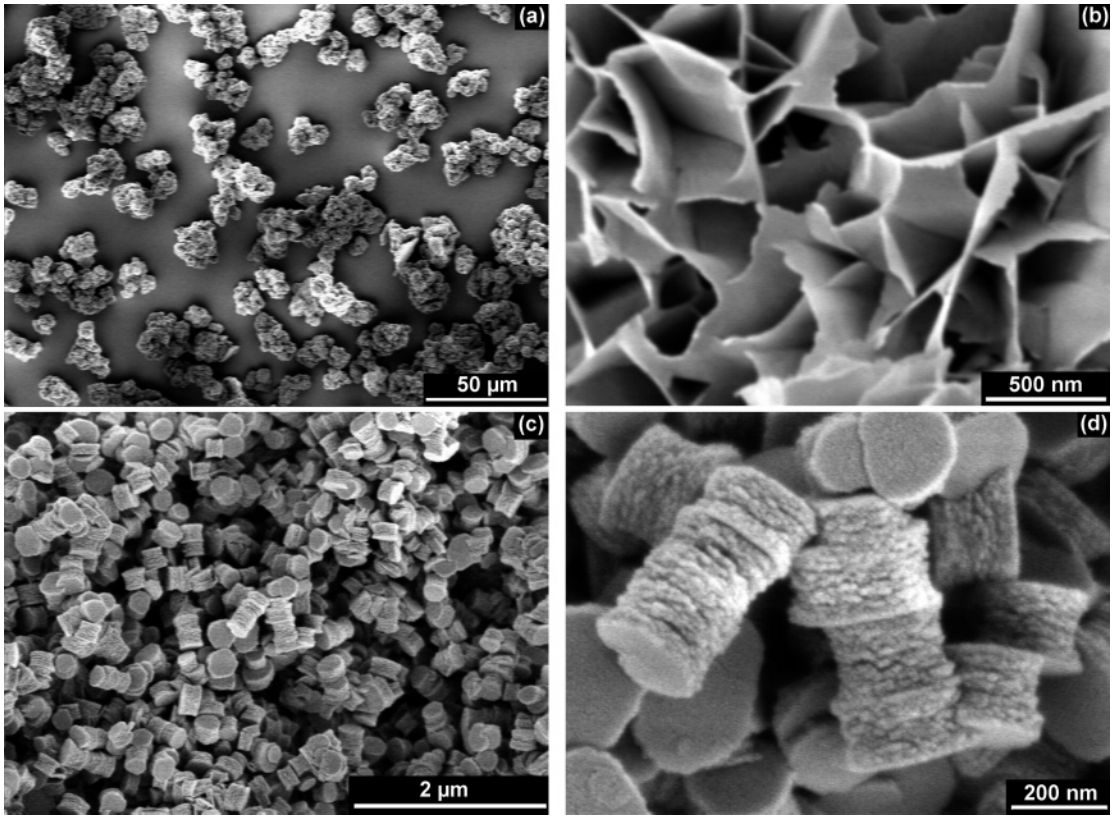

Figure 2. SEM micrographs of the control sample (a, b) and of nickel hydroxide β-Ni(OH)$_2$ (sample A) precipitated by ammonia decomplexation (c, d).

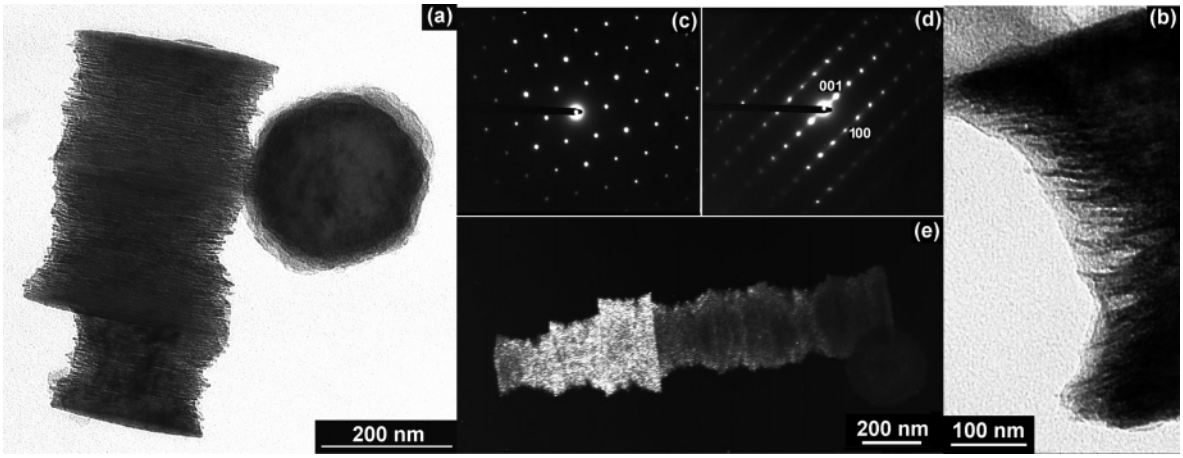

Figure 3. Bright field images (a, b), corresponding to selected area electron diffractions SAED of front view stacks (c) and side view stacks (d), and dark field TEM micrographs (e) of nickel hydroxide β-Ni(OH)$_2$ (sample A) precipitated by ammonia decomplexation.

plane of the hexagonal β phase. SAED performed on the side of the stacks (Figure 3d) corroborates that the (001) direction is the axis of revolution of each cylinder. Furthermore, single point diffraction patterns indicate a high degree of crystallization and orientation within a single particle.

Such a homogeneity is also emphasized by dark field (DF) images performed on particles deposited on their side. A single diffracted beam, indexed as (001) in Figure 3d, is selected in order to form the TEM image (Figure 3e). All regions of the sample not displaying the same crystal orientation as the region that produced the selected diffracted beam appeared very dark in the DF image. As shown in Figure 3e, each stack, bright or dark depending on the Bragg condition at a certain angle, displays quasiuniform brightness.

Two synthesis parameters were investigated: the added amount of ammonia and the bulk temperature during the addition of ammonia. We particularly focus on crystalline and morphological changes.

The Amount of NH_3. Four experiments were performed with different amounts, X_{NH_3}, of ammonia diluted in 400 mL of distilled water: 60, 80, 120, and 160 mL (0.88, 1.17, 1.76, and 2.35 mol of NH_3, respectively). In this section, the reaction medium was heated at 60 °C immediately after the base addition.

As was made clear by XRD (Figure 4a−c), the well-crystallized β-Ni(OH)$_2$ is obtained when the ammonia amount ranges from 60 to 120 mL. Moreover, the sizes of the crystalline domain along the *c*-axis (L_{001}) and along the (110) direction (L_{110}), calculated applying the Scherrer's formula (Table 1), are similar for $X_{NH_3} = 60$ mL ($L_{001} = 50$ nm and $L_{110} = 36$ nm) and for $X_{NH_3} = 80$ mL ($L_{001} = 50$ nm and $L_{110} = 36$ nm). When X_{NH_3} is equal to 120 mL, L_{001} is divided by two (26 nm), whereas L_{110} slightly decreases to 30 nm. Thus, by increasing the amount

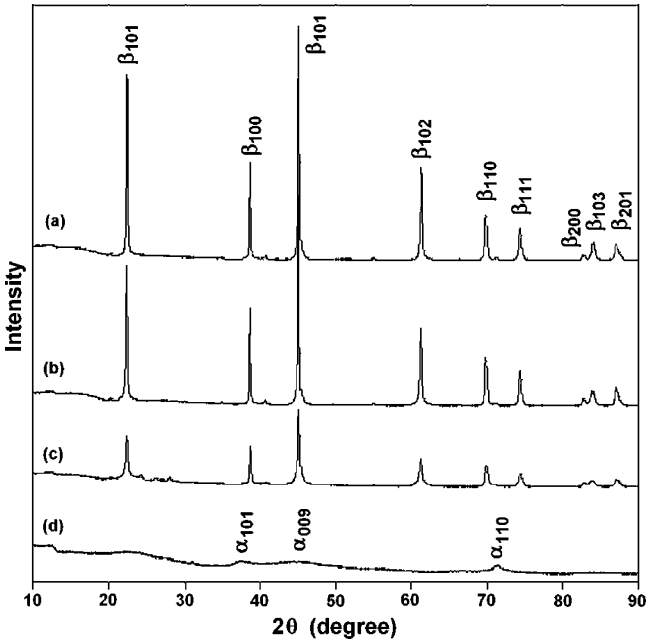

Figure 4. Powder X-ray diffraction patterns of nickel hydroxides Ni(OH)$_2$ precipitated by ammonia decomplexation for $X_{NH_3} = 60$ (a), 80 (b), 120 (c), and 160 mL (d).

of complexing base, the crystalline domain size is lowered until the turbostratic α-Ni(OH)$_2$ for $X_{NH_3} = 160$ mL (Figure 4d) is obtained. In this case, crystal domains are sharply reduced as $L_{001} = 2$ nm and $L_{110} = 10$ nm (Table 1). Meyer et al.[15] synthesized Ni(OH)$_2$ platelets for different amounts of NH_3 and observed that the crystal sizes deduced from XRD patterns slightly increase for $R = [NH_3]/[Ni]$ increasing from 2 up to 20. The influence of base content also exists in our study for higher values of R (ranging from 18 to 48), but in the presence of nickel functionalized surfactant.

TEM observations (Figure 5) reveal the influence of NH_3 content on both shape and size (Table 1) of the synthesized hydroxides. The higher X_{NH_3}, the larger the characteristic size of the particles, and the less regular the stacking mode for β-Ni(OH)$_2$. For $X_{NH_3} = 60$ mL, the measured mean diameter is about 374 nm and the mean thickness around 114 nm. For $X_{NH_3} = 80$ mL, the cylinders have a bigger diameter and are twice as thick, displaying a median constriction. For $X_{NH_3} = 120$ mL, no well-defined shape remains so that no particle size could be evaluated on TEM micrographs. On the other hand, α-Ni(OH)$_2$ synthesized at $X_{NH_3} = 160$ mL consists of rods the length of which is roughly 600 nm with a diameter of about 100 nm. SEM analysis (Figure 6) completes the characterization of synthesized α-Ni(OH)$_2$, revealing that the sample exclusively consists of submicronic rods.

The Temperature of the Base-Addition Step. The same experiment as described in the first section ($X_{NH_3} = 80$ mL) was carried out, except that during the whole synthesis, the temperature was fixed at 60 °C. According to XRD analysis, well-crystallized β nickel hydroxide was obtained, and the sizes of the crystal domain were estimated at 48 nm for L_{001} and 38 nm for L_{110}. These lengths are similar to those obtained in the cases of $X_{NH_3} = 60$ and 80 mL and slightly smaller than those of sample A. As is made clear by TEM characterization (Figure 7), the "stack of pancakes" morphology remains, and the particle diameter is roughly the same (320 ±80 nm), whereas the thickness is divided by two (86 ±16 nm) in comparison with sample A (Table 1). Such a result underlines the influence of the purple solid obtained during base addition on the external shape of final particles. In fact, this experiment only differs by the temperature of the base addition step, which has no impact on the lamellar structure but on the stacking length.

Discussion

To underline the benefit from surfactant functionalization, another control experiment was performed with a mixture of nickel sulfate salt ($NiSO_4$, 0.05 mol) and sodium dodecyl sulfate (SDS, 0.10 mol) instead of nickel dodecyl sulfate (Ni(DS)$_2$). The mere addition of surfactant in the bulk furthers a "stack of pancakes" morphology. However, the shape and the size distribution of the particles are significantly less homogeneous. The difference between both methods lies in the presence or not of sodium sulfate in the medium, hence the deterioration in pancakes crystallization is due to the competition between the actions of sulfate and dodecyl sulfate: sulfate may hinder the templating role of dodecyl sulfate by adsorption on nickel hydroxide surfaces. This problem is avoided in the case of surfactant functionalization that eliminates all anions except templating dodecyl sulfate and reacting hydroxides.

Surfactant has a role on nucleation and crystal growth during precipitation, but questions on the detailed nucleation mechanism and surfactant−complexing agent (ammonia) interactions remain. To our knowledge, this morphology is original with nickel hydroxides and it was found interesting to draw a parallel with other kinds of particles exhibiting similar morphologies. Lamellar morphology was obtained in the case of polymer-mediated mineralization of zinc oxide in aqueous solution.[16−18] Diblock copolymers were used to control particle's morphology, size, and size distribution. The use of poly(ethylene oxide-*block*-styrene sulfonic acid) (P(EO-*b*-SSH)) led to uniform 1-μm stacks. Actually, a highly ordered single crystalline core might appear first. Then, the copolymer, released as a metastable intermediate was dissolved, seemed to adsorb onto the side faces of the growing crystal. Hence, growth could only occur where the polymer was not adsorbed, giving rise to lamellae of about 10 nm. Finally, a "corn on a cob" structure was more accurate to describe the precipitate.[16,18]

In our case, the question of the real nature of the inner structure also needs to be clarified. On one hand, a difference

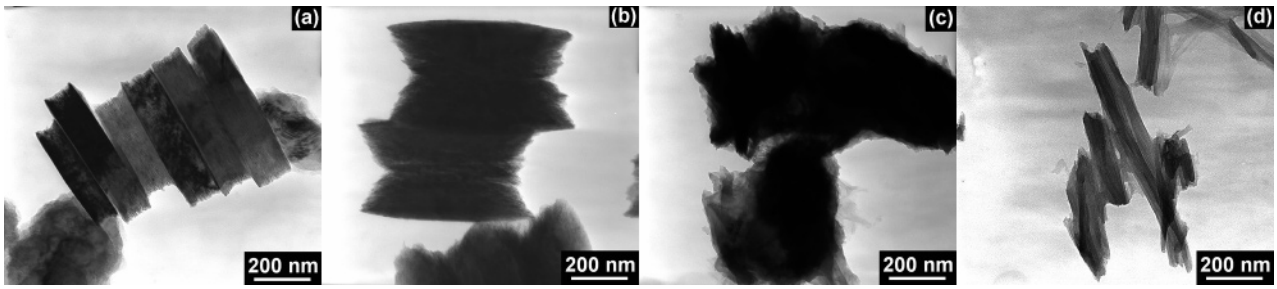

Figure 5. Scanning electron micrographs of nickel hydroxides Ni(OH)$_2$ precipitated by ammonia decomplexation for $X_{NH_3} = 60$ (a), 80 (b), 120 (c), and 160 mL (d) (same magnification).

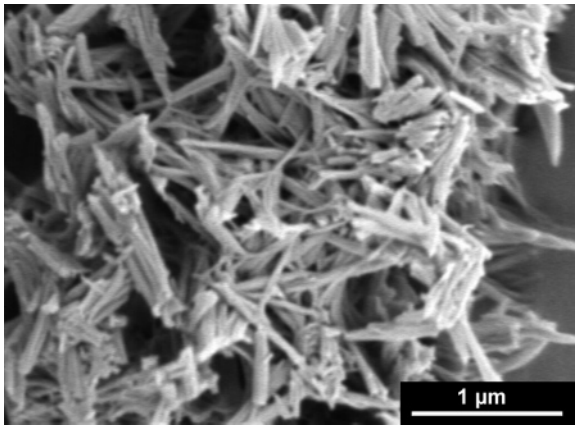

Figure 6. Scanning electron micrograph of α nickel hydroxide obtained by ammonia decomplexation for $X_{NH_3} = 160$ mL.

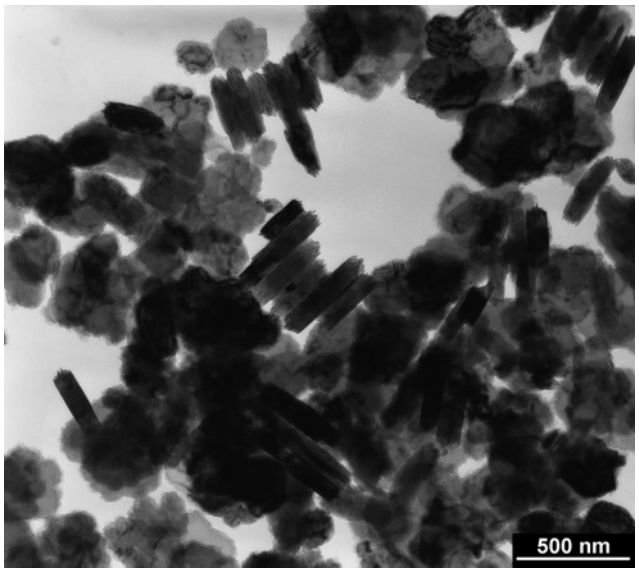

Figure 7. Bright field TEM micrograph of nickel hydroxide β-Ni(OH)$_2$ precipitated by ammonia decomplexation with a base addition step at 60 °C.

lies in the intrinsic crystal nature of ZnO and Ni(OH)$_2$. First, ZnO precipitated without polymer consists of large hexagonal prisms (1 μm in width and a few micrometers long) resulting from a favored growth along the polar *c*-axis. That could account for an elongated single crystalline inner part holding the lamellae in the case of polymer-mediated synthesis. In contrast, nickel hydroxide exhibits a crystal lamellar feature characterized by Ni(OH)$_2$ slabs built up of NiO_6 edge-sharing octahedra, and generally displays 2D structure. By employing strong base, hexagonal platelets displaying 200-nm diameter are obtained, or homogeneous ammonia decomplexation leads to nanometric plates[15] or to micrometric particles consisting of thin and large branched platelets, as illustrated by the sulfate control sample (Figure 2b). These platelets whose thickness varies between 10 and 40 nm could be shaped, made thinner, and assembled by template agents. Moreover, the adsorption mechanism of the diblock copolymer is different from that of smaller surfactant molecules such as SDS. The first one preferentially adsorbs on the surface via the P(SSH) blocks whereas the P(EO) ones remain in solution as a random polymer coil inducing lamellae growth in the free space. The C_{12} chain of dodecyl sulfate is not expected to build such a comblike template. Dodecyl sulfate is still present in the obtained particles (checked by IR spectroscopy), but at this stage we could not discriminate

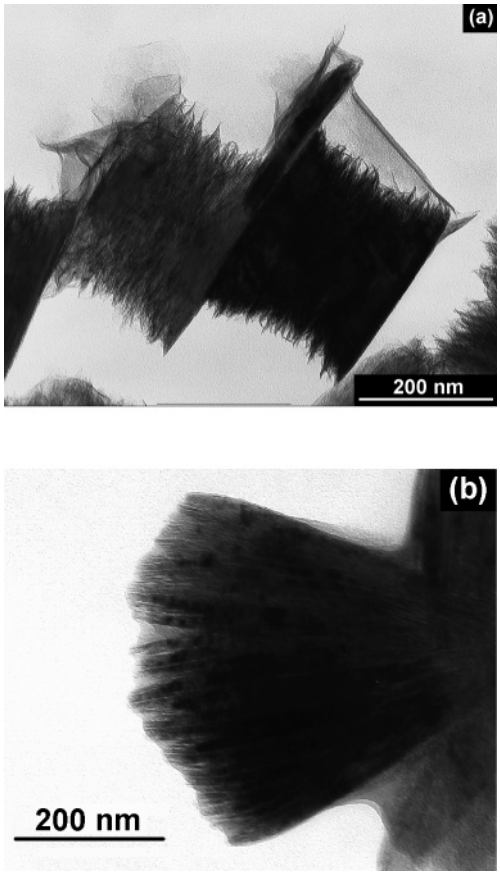

Figure 8. Discussion on the inner structure of a stack. Bright field TEM micrographs of nickel hydroxide β-Ni(OH)$_2$ precipitated by ammonia decomplexation: after aging in distilled water for several months (a) and displaying a fanlike particle (b).

between dodecyl sulfate adsorbed on the external surface and the apparent lamellae. However, the specific surface area was calculated by applying the Brunauer−Emmet−Teller (BET) model on nitrogen adsorption/desorption isotherms measured at 77 K, using a Micromeritics ASAP2010 model. The BET specific surface area of sample A was evaluated at 7 $m^2 \cdot g^{-1}$. This low surface may be due to the fact that thin lamellae exist only near the surface since such a value is similar to the surface displayed by smooth cylinders 300 nm in diameter and 200 nm in width (5.9 $m^2 \cdot g^{-1}$), or to the filling of interlamellar space by surfactant. Organic species were removed by calcination (400 °C during 6 h), and the resulting NiO particles exhibited the same morphology as hydroxides with a higher specific surface area (128 $m^2 \cdot g^{-1}$) that squares with the calculated area of platelets 300 nm in diameter and 2.5 nm in width (120 $m^2 \cdot g^{-1}$). Besides the fact that surfactant did not evacuate the interplatelet space in hydroxide, such a result strengthens that lamellae represent an important part of the particles, so they are not only a phenomenon localized near the particle surface, and the relevancy of a "stack of pancakes" model to describe the observed morphology. In addition, a part of the sample remained several months in distilled water, then was examined by TEM (Figure 8a). Thin layers clearly came unstuck from the surface of one particle. Moreover, the presence of a cross slice should result from the diminution of interlayer cohesion, and could not appear if all layers were connected to a single crystal central spine. On the other hand, the integrity of particles is globally maintained, which was also verified in ethanol. Hence, a mechanism involving oriented attachment of platelets in perfect parallel orientation with respect to the others and partial

recrystallization in the core of the particles could give rise to large coherence lengths. On the other hand, single-crystal core carrying lamellae would be consistent with single point diffraction patterns obtained by TEM. Moreover, both the shape and the width of XRD peaks may lean toward the presence of a single-crystal core. Indeed, when stacks were obtained, the length L_{001} along the *c*-axis ranges from 26 to 54 nm, which is widely superior to 3.5 nm corresponding to a single layer measured on TEM micrographs. Between the two extreme cases (one central monocrystalline spine with comblike surface and the perfectly oriented attachment of nanodisks), intermediate cases would tally with our observations, for example, comblike building blocks having a thickness consistent with (001) coherence lengths (a few tens of nanometers) and stacking together with perfectly oriented attachment. This hypothesis may be consistent with the observation of some fanlike particles that seem to be regularly divided in slices about 40 nm, themselves consisting of 4 nm lamellae stacking (Figure 8b). Once stacks of pancakes synthesized, it looks as if the stacking mode also occurs in a superior scale as final cylinders line up forming the chain, whcih could be another relevant point to the "stack of pancakes" and oriented attachment assumptions.

Sticking to the nickel hydroxide system, results that can be related to ours are scarce. Sac Epée et al.[19] prepared β(III) and γ(III) nickel oxyhydroxides to study their reduction in the presence of hydrogen. The precursor α-$Ni(OH)_2$ was obtained by adding $Ni(NO_3)_2$ to ammonia, and processed into β-$Ni(OH)_2$ under hydrothermal conditions (125 °C, 6 h). Then, β(II) nickel hydroxide was oxidized with NaClO and KOH at 80 °C resulting in pure γ(III) nickel oxyhydroxide. Among angular platelets ranging from 100 to 200 nm, the presence of a 180 nm diameter "stack of pancakes" was revealed by TEM. Hydrothermal settings seem to be favorable for the emergence of the layered stacking arrangement. Besides crystallinity considerations, it is intriguing to note this second similarity between particles resulting from our low temperature method and hydrothermal synthesis. Furthermore, bearing in mind that stacks can be observed lying either on the (001) plane or perpendicularly along the *c*-axis, discriminating between thin stacks on the edge and nanorods may prove tricky in certain cases. Li et al.[20] reported a direct conversion method from nickel oxalate NiC_2O_4 into nanoflakes and nanorods of $Ni(OH)_2$ in NaOH solution at 160 °C for 12 h. Liang et al.[21] further observed the coexistence of nanoflakes and nanorods, employing nickel acetate $Ni(CH_3COO)_2$ and ammonia by the hydrothermal method (200 °C for 2 h). As a consequence, one can wonder if the apparent juxtaposition of both morphologies may correspond to the side view and the front view of the unique "stack of pancakes" morphology.

Acknowledgment. The authors are most grateful to François Grillon for having performed high-quality scanning electron micrographs despite the difficulty resulting from the intrinsic nature of hydroxides. Thanks are also due to Erika Canavin, who took an active part in the achievement of experiments during her training period.

References and Notes

(1) Taniguchi, A.; Fujioka, N.; Ikoma, M.; Ohta, A. *J. Power Sources* **2001**, *100*, 117.
(2) Shukla, A. K.; Venugopalan, S.; Hariprakash, B. *J. Power Sources* **2001**, *100*, 125.
(3) Morioka, Y.; Narukawa, S.; Itou, T. *J. Power Sources* **2001**, *100*, 107.
(4) Boschloo, G.; Hagfeldt, A. *J. Phys. Chem. B* **2001**, *105*, 3039.
(5) Le Bihan, S.; Figlarz, M. *J. Cryst. Growth* **1972**, *13/14*, 458.
(6) Oliva, P.; Leonard, J.; Laurent, J. F.; S. A. F. T.; Delmas, C.; Braconnier, J. J.; Figlarz, M.; Fievet, F.; de Guibert, A. *J. Power Sources* **1982**, *8*, 229.
(7) Le Bihan, S.; Guenot, J.; Figlarz, M. *C. R. Acad. Sci. Paris* **1970**, *270*, 2131.
(8) Braconnier, J. J.; Delmas, C.; Fouassier, C.; Figlarz, M.; Baudouin, B.; Hagenmuller, P. *Rev. Chim. Miner.* **1984**, *21*, 496.
(9) Genin, P.; Delahaye-Vidal, A.; Portemer, F.; Tekaia-Elhsissen, K.; Figlarz, M. *Eur. J. Solid State Inorg. Chem.* **1991**, *28*, 505.
(10) Yang, D.; Wang, R.; Zhang, J.; Liu, Z. *J. Phys. Chem. B* **2004**, *108*, 7531.
(11) Akinc, M.; Jongen, N.; Lemaître, J.; Hofmann, H. *J. Eur. Ceram. Soc.* **1998**, *18*, 1559.
(12) Soler-Illia, G. J. d. A. A.; Jobbágy, M.; Regazzoni, A. E.; Blesa, M. A. *Chem. Mater.* **1999**, *11*, 3140.
(13) Feltin, N.; Pileni, M. P. *Langmuir* **1997**, *13*, 3927.
(14) Delmas, C.; Tessier, C. *J. Mater. Chem.* **1997**, *7* (8), 1439.
(15) Meyer, M.; Bée, A.; Talbot, D.; Cabuil, V.; Boyer, J. M.; Répetti, B.; Garrigos, R. *J. Colloid Interface Sci.* **2004**, *277*, 309.
(16) Taubert, A.; Kübel, C.; Martin, D. C. *J. Phys. Chem. B* **2003**, *107*, 2660.
(17) Taubert, A.; Palms, D.; Weiss, Ö.; Piccini, M.-T.; Batchelder, D. N. *Chem. Mater.* **2002**, *14*, 2594.
(18) Taubert, A.; Glasser, G.; Palms, D. *Langmuir* **2002**, *18*, 4488.
(19) Sac Epée, N.; Beaudoin, B.; Pralong, V.; Jamin, T.; Tarascon, J.-M.; Delahaye-Vidal, A. *J. Electrochem. Soc.* **1999**, *146* (7), 2376.
(20) Li, X. L.; Liu, J. F.; Li, Y. D. *Mater. Chem. Phys.* **2003**, *80*, 222.
(21) Liang, Z.-H.; Zhu, Y.-J.; Hu, X.-L. *J. Phys. Chem. B* **2004**, *108*, 3488.